Title: A Chemical Shift Encoding (CSE) Approach for Spectral Selection in Fluorine-19 MRI
Authors: Kai D. Ludwig, Diego Hernando, Nathan T. Roberts, Ruud B. van Heeswijk, Sean B. Fain
Journal: Magnetic Resonance in Medicine
Year: 2017
Volume:
Issue:
Pages:
DOI: 10.1002/mrm.26874

A Chemical Shift Encoding (CSE) Approach for Spectral Selection in Fluorine-19 MRI

Kai D. Ludwig[1], Diego Hernando[1,2], Nathan T. Roberts[2,3], Ruud B. van Heeswijk[4], Sean B. Fain*[,1,2,5]

[1]Medical Physics, University of Wisconsin, Madison, WI, USA
[2]Radiology, University of Wisconsin, Madison, WI, USA
[3]Electrical and Computer Engineering, University of Wisconsin, Madison, WI, USA
[4]Radiology, Lausanne University Hospital (CHUV) and University of Lausanne (UNIL), Lausanne, Switzerland
[5]Biomedical Engineering, University of Wisconsin, Madison, WI, USA

*Corresponding Author: Sean B. Fain, PhD, 1111 Highland Avenue, Room 1133 Wisconsin Institutes for Medical Research, University of Wisconsin-Madison, Madison, WI 53705-2275; Phone 608-262-2170; Fax 608-262-2413; e-mail sfain@wisc.edu

Running Title: Chemical Shifting Encoding ^{19}F MRI

Word Count: 3310

Acronyms: **^{19}F** = fluorine-19, **CRLB** = Cramér-Rao lower bound, **CSE** = chemical shift encoding, **FFT/iFFT** = fast Fourier transform/ inverse fast Fourier transform, **FOV** = field-of-view, **ISO** = isoflurane, **MRI** = magnetic resonance imaging, **NSA_{eff}** = effective number of signal averages, **PFCE** = perfluoro-15-crown-5-ether, **RF** = radiofrequency, **rBW** = receiver bandwidth, **SNR** = signal-to-noise ratio, **TE** = echo time, **TE_{init}** = initial echo time, **N_{TE}** = number of echo times, **TR** = repetition time

Key words: fluorine-19, magnetic resonance imaging, chemical shift encoding

Abstract

Purpose: To develop a chemical shift encoding (CSE) approach for fluorine-19 (^{19}F) MRI of perfluorocarbons in the presence of multiple known fluorinated chemical species.

Theory and Methods: A multi-echo CSE technique is applied for spectral separation of the perfluorocarbon perfluoro-15-crown-5-ether (PFCE) and isoflurane (ISO) based upon their chemical shifts at 4.7 T. Cramér-Rao lower bound (CRLB) analysis is used to identify echo combinations with optimal signal-to-noise performance. Signal contributions are fit with a multispectral fluorine signal model using a non-linear least squares estimation reconstruction directly from k-space data. This CSE approach is tested in ^{19}F phantoms and in a mouse with a 2D and 3D spoiled gradient-echo acquisition using multiple echo times determined from CRLB analysis.

Results: CRLB analysis for PFCE and ISO separation shows signal-to-noise performance is maximized with a 0.33 ms echo separation. A linear behavior (R^2 = 0.987) between PFCE signal and known relative PFCE volume is observed in CSE reconstructed images using a mixed PFCE/ISO phantom. Effective spatial and spectral separation of PFCE and ISO is shown in phantoms and in vivo.

Conclusion: Feasibility of a gradient-echo CSE acquisition and image reconstruction approach with optimized noise performance is demonstrated through ^{19}F MRI of PFCE with effective removal of ISO signal contributions.

Introduction

Fluorine-19 (^{19}F) MRI is a highly specific and quantitative technique for cellular and molecular detection. MRI of biocompatible ^{19}F contrast agents, such as perfluorocarbons, has shown immense promise for visualization of inflammation events as well as monitoring immune and stem cell populations in preclinical animal models (1, 2). Fluorinated anesthetics (e.g. isoflurane) are commonly used in longitudinal preclinical applications due to the fast induction and recovery time, ease-of-use and flexibility in different procedural environments, and minimal toxicity. Being an inhaled halogenated ether, isoflurane introduces substantial background signal (3, 4), which complicates the interpretation of ^{19}F images. Furthermore, the resonant frequencies of isoflurane's spectral groups may overlap with those of several fluorinated contrast agents (5, 6). For these reasons, removal of isoflurane signal from ^{19}F images is highly desirable.

The quantification of fluorine concentrations in vivo among others relies on the specificity of the fluorine signal that originates from the contrast agent only. Current approaches for ^{19}F MR imaging in the presence of fluorinated anesthetics have often assumed negligible fluorine signal contamination from anesthetics. However, confounding anesthetic signal may obfuscate results, particularly in anatomical regions of high isoflurane uptake, e.g. peritoneal, thoracic, and cranial cavities (4, 7, 8). While certain injectable anesthetics (e.g. ketamine/xylazine) would not contribute background signal, access to the controlled substance, ketamine, is limited and requires a DEA license in the United States. Further, injectable anesthetics are not easily titrated within the MR environment and may require an infusion pump, all of which are not conducive for longitudinal preclinical studies. One strategy for removing confounding fluorine-19 background signals is to characterize the anesthetics accumulation in vivo (5) to determine the spatial overlap with contrast agents, while another is to confine radiofrequency (RF) excitation and/or signal saturation to the desired chemical species by introducing narrow-frequency Gaussian-filtered RF excitation pulses (3). However, frequency-selective RF excitation approaches may fail in the presence of large susceptibility variations. Further, signal suppression methods tend to suffer from longer scan times and reduced image signal-to-noise ratio (SNR).

Recent advances in model-based chemical shift encoding (CSE) techniques (9, 10) exploit a priori knowledge of the resonant frequency separations between chemical species as image reconstruction constraints. Such CSE techniques enable chemical species separation

with high SNR-efficiency, and are widely used for fat/water separation in ^{1}H MRI (9, 11-14). These techniques are based on the acquisition of multiple images, each with a different echo time (TE), followed by model-based reconstruction to separate the various chemical species. Common Dixon techniques (15-17) rely on image space-based separation of chemical species, which is often acceptable for fat/water separation. For instance, the chemical shift separation seen for water and fat resonances is on the order of hundreds of Hz at clinical field strengths, leading to modest chemical shift artifacts with most (e.g. Cartesian) acquisitions. However, due to the wide chemical shift separation between fluorine peaks in ^{19}F MRI (on the order of thousands of Hz at 4.7 T), significant phase accumulation occurs during the acquisition trajectory, leading to substantial chemical shift artifacts in the presence of multiple fluorine species and incorrect specie separation using image space methods. Thus, the image-space methods are inadequate for ^{19}F CSE. Instead, a generalized k-space model-based CSE reconstruction is needed, similar to the approach proposed by Brodsky et al. (18). This k-space signal modeling CSE approach corrects the significant phase accumulation during the imaging readout and allows for flexible choice of initial echo time (TE_{init}), echo spacing (ΔTE), number of echo times (N_{TE}), and sampling trajectory.

In this work, we therefore propose a CSE approach that can be used to separate the ^{19}F signal from multiple fluorine-19 species. We demonstrate utility by separating signal arising from perfluorocarbon contrast agents from that of anesthetics based on their unique ^{19}F spectrum. This CSE approach is implemented to separate perfluoro-15-crown-5-ether (PFCE) from isoflurane (here-after referred to as ISO), while its signal-to-noise performance is optimized through numerical simulations. Finally, we evaluate the proposed CSE method using both 2D and 3D spoiled gradient-echo acquisitions in phantoms and in vivo.

Theory

We propose a multiple gradient echo CSE acquisition with images acquired at different echo times (TE). The acquired data are processed using non-linear least-squares estimation to directly reconstruct the PFCE, $\rho_P(x,y,z)$, and isoflurane, $\rho_I(x,y,z)$, images from the acquired k-space data. The signal model (Eq. 1) includes the resonant frequencies of the PFCE peak, f_P, and M additional spectral (e.g. isoflurane) peaks, f_m, with relative signal amplitude, α_m (for $m = 1, \dots, M$), the frequency shift, $\Delta f_B(x,y,z)$, due to local B_0 field inhomogeneity and phase evolution during the time-dependent frequency encoding readout, $k_y(t)$, where t is the time relative to the TE during the readout.

$$s_{TE}(k_x, k_y, k_z, t; \Delta f_B, \rho_P, \rho_I) =$$

$$\iiint_{x,y,z} e^{i2\pi\cdot(\Delta f_B[TE+t]+k_x x+k_y(t) y+k_z z)} \cdot \left(\rho_P \cdot e^{i2\pi f_P[TE+t]} + \rho_I \cdot \sum_{m=1}^{M} \alpha_m e^{i2\pi f_m[TE+t]}\right) dxdydz \quad [1]$$

For conciseness, the spatial dependence of the parametric maps $\rho_P(x,y,z)$, $\rho_I(x,y,z)$, and $\Delta f_B(x,y,z)$ was omitted from the signal model. We have assumed negligible contribution from T_2* in the above signal model when using a TE < 5 ms for all MR acquisitions. Non-localized ^{19}F spectroscopy was used to measure f_P and the multiple f_m peaks prior to acquisition of ^{19}F CSE MR data. These are then input into Eq. 1 as frequency shifts relative to f_P, which corresponds to the acquisition transmit frequency (~0 Hz).

The proposed reconstruction is based on direct non-linear least-squares estimation from k-space. For computational efficiency, the k_z dimension (which is phase encoded and does not suffer from chemical shift artifacts) was Fourier transformed into image space, and the reconstruction was performed separately for each z location. In principle, the phase-encoded k_x dimension could also be reconstructed directly leading to a 1D problem for each (x,z) location. However, in the proposed method the reconstruction was performed in 2D (x,y) space, to improve field map estimation by incorporating field map smoothness regularization in 2D (rather than just 1D). In summary, the proposed reconstruction (Eq. 2) minimizes the difference between the measured k-space signal (s_{meas}) and the signal model in Eq. 1, to reconstruct the three unknown parametric maps $\rho_P, \rho_I, \Delta f_B$.

$$[\Delta f_B, \rho_P, \rho_I] = \underset{\Delta f_B, \rho_P, \rho_I}{\arg\min} \|s_{\text{meas}} - s_n(\Delta f_B, \rho_P, \rho_I)\|^2$$
$$\text{where} \quad \Delta f_B(x,y) = \sum_{n=1}^{N} \beta_n \varphi(x,y) \quad [2]$$

Specifically, the reconstruction for each z location is constrained by assuming a spatially smooth main magnetic field where the estimated field map Δf_B is constrained to be a linear combination of smooth sinusoidal basis functions in 2D, $\varphi(x,y)$ with relative amplitude, β_n.

Methods

Noise performance optimization: Cramér-Rao lower bound (CRLB) analysis (19) was performed to determine the signal-to-noise performance of the image reconstruction using different combinations of TE_{init} and ΔTE for a set number of echo times (N_{TE}). Here, we use the number of signal averages (NSA), defined as the variance in a source image (image reconstructed by

direct iFFT of k-space data and averaged in the echo dimension) divided by the variance in a CSE reconstructed image, as the metric for noise performance. CRLB analysis was repeated for several different N_{TE} and in order to appropriately compare results, NSA was normalized to the N_{TE} to equal the theoretical effective number of signal averages (NSA_{eff}). CRLB analysis assumed a transmit frequency centered on the PFCE resonance frequency (f_{PFCE} = 0 Hz).

Phantom experiments: All MR data were acquired on a 4.7 T preclinical MRI system (Agilent Technologies, Santa Clara, CA) using a custom-built quadrature volumetric RF coil tunable to either the ^{1}H (100 MHz) or the ^{19}F (188 MHz) frequencies. The RF coil was tuned and matched to the ^{1}H frequency for shimming, localization, and relevant MRI sequences. Next, the coil was manually re-tuned and matched to the ^{19}F frequency for ^{19}F MRI sequences. The transmit frequency for all ^{19}F MR experiments was centered on PFCE's resonance frequency. Two phantoms were created by filling 0.5 mL micro-centrifuge tubes with either PFCE (Exfluoro, Round Rock, TX) or ISO (Piramal, Bethlehem, PA). The ^{19}F chemical shift separation between f_P and the multiple f_m peaks were measured from an MR spectrum collected with a 90° non-selective excitation, receiver bandwidth (rBW) = 10 kHz, and acquired signal averages = 1 in the phantoms and used as frequency inputs in the signal model (Eq. 1) and CSE image reconstruction. The feasibility of the CSE technique was demonstrated in these two phantoms using a ^{19}F 2D spoiled gradient-echo acquisition with a single TE per repetition time (TR) repeated N_{TE} times (TR/TE_{init}/ΔTE = 20.0/2.8/0.33 ms, N_{TE} = 6, matrix = 128x128, field-of-view (FOV) = 48x48 mm^2, a single 2 mm slice, rBW = 50 kHz, flip angle = 20°, and signal averages = 1, scan duration = 41 s). To observe the effect of the B_0 field correction, CSE reconstruction was performed both with and without the Δf_B term from Eq. 1 using the ^{19}F gradient-echo data.

In a second, quantitative comparison, micro-centrifuge tubes with mixed relative volumes of PFCE and ISO (volumes of PFCE/ISO: 700/0, 525/175, 350/350, 175/525, and 0/700 µL) were prepared for a total ~700 µL volume. A 3D printed holder supported the micro-centrifuge tubes within the RF coil. The mixed relative volume phantom was subsequently imaged using a 3D spoiled gradient-echo acquisition with a single TE per TR repeated N_{TE} times with acquisition parameters optimized for chemical shift separation and high signal-to-noise through CRLB analysis (TR/TE_{init}/ΔTE = 10.0/2.3/0.33 ms, N_{TE} = 6, matrix = 96x96x24, FOV = 32x32x48 mm^3, rBW = 30 kHz, flip angle = 10°, signal averages = 1, scan duration = 2 min 18 s). For one signal average, the resulting acquisition time per image for a given TE was 23 s.

In vivo experiment: To demonstrate feasibility of CSE image reconstruction in vivo, MR data was collected in one healthy, male, C57BL/6 mouse anesthetized with 1.5% isoflurane and maintained at 36.5 ± 0.5°C throughout MR imaging using a temperature probe and hot-air blower. This pilot study complied with institutional animal care and use committee regulations. A biocompatible PFCE emulsion was synthesized as a kinetically stable, oil-in-water nanoemulsion loaded with PFCE. A ^{19}F MR spectrum was acquired, to determine the in vivo ^{19}F chemical shifts and subsequently used in the signal model (Eq. 1) and image reconstruction. ^{19}F MRI data was acquired with a 3D spoiled gradient-echo acquisition with a single TE per TR repeated N_{TE} times using the chosen TE_{init} and ΔTE combination from the CRLB analysis and confirmed empirically in the phantom experiments ($TR/TE_{init}/\Delta TE$ = 200/2.3/0.33 ms, N_{TE} = 6, matrix = 48x24x8, FOV = 80x40x32 mm^3, rBW = 18 kHz, flip angle = 20°, signal averages = 8, scan duration = 30 min 43 s). For one signal average, the resulting acquisition time per image for a given TE was 39 s. However, eight signal averages were acquired in vivo based on empirical performance to achieve sufficiently high signal-to-noise to observe background signal from ISO uptake. Spectra and images were acquired prior to and after intraperitoneal injection of 45 mM of a PFCE emulsion. Anatomic ^{1}H MR data was acquired with a T_2-weighted 2D fast spin echo sequence (TR/ΔTE = 4431.6/16.5 ms, echo train length = 8, matrix = 256x128, FOV = 80x40 mm^2, spatial resolution = 0.31x0.31 mm^2 in-plane with 1 mm slice thickness, rBW = 100 kHz, signal averages = 3, scan duration = 3 min 33 s). ^{19}F MR images were up-sampled to match the matrix dimensions of ^{1}H MR images. The B_0 field map was estimated in vivo using a separate ^{1}H 2D spoiled gradient echo acquisition ($TR/TE_{init}/\Delta TE$ =103.5/4.2/0.4 ms, N_{TE} = 6, matrix = 256x128, FOV = 80x40 mm^2, with 2 mm slice thickness, rBW = 78 kHz, flip angle = 20°, signal averages = 8, scan duration = 14 min 8 sec).

All simulations, image reconstructions, and data analyses were performed in Matlab 2014b (MathWorks, Natick, MA). To determine the performance of the CSE-reconstructed images, they were compared to images that were reconstructed separately by direct iFFT of the k-space data and averaged in the echo dimension. These images will be referred to as ‘source’ images.

Results

The relative chemical shifts between the two spectral groups of ISO (CF_3 and CHF_2) and the singular peak of PFCE at 4.7 T were 1.8 kHz (9.6 ppm) and 0.45 kHz (2.4 ppm) in vitro, respectively (Fig. 1a). Variable signal was seen in the ISO phantom as a result of the spectral groups being in- and out-of-phase in the iFFT reconstructed MR images at different TEs (Fig.

1b). Chemical shift artifact was also observable in the physically aligned PFCE and ISO phantoms. Using the chemical shift separations between the fluorine peaks, CRLB analysis provided data acquisition parameters (TE_{init} = 2.8 ms for 2D and 2.3 ms for 3D, ΔTE = 0.33 ms, and N_{TE} = 6) that maximized the theoretical NSA_{eff} for the given fluorinated chemical species (Fig. 2). Note that while increasing the N_{TE} included in the CRLB analysis enlarges the regions with very high NSA_{eff} (>0.95), an inevitable tradeoff is prohibitively long scan times. The acquisition time per image with 8 signal averages for a given TE was 5 min 7 s. Six TEs were therefore chosen for subsequent CSE acquisitions in phantoms and in vivo experiments as a balance between high NSA_{eff} and scan time. The TE_{init} values between the 2D and 3D spoiled gradient-echo sequences, as noted accordingly in Figure 2, were selected based on the minimum achievable TE for the pulse sequence, which also coincided with regions of high NSA_{eff} (>0.95) further improving the acquisition efficiency. The NSA_{eff} values from CRLB were 0.99 and 0.97 for the selected 2D and 3D acquisition parameters optimized in this way, respectively. The NSA_{eff} was normalized to the N_{TE} so the reported NSA_{eff} values are less than or equal to 1.

Feasibility of the CSE reconstruction of separate PFCE and ISO ^{19}F images was demonstrated in phantoms of 100% PFCE and 100% ISO (Fig. 3). The CSE reconstruction spatially and spectrally resolved both fluorine species while eliminating artifacts arising from chemical shift and B_0 field inhomogeneity. The inclusion of the B_0 field estimate in the signal model reduced PFCE signal 'leakage' into the ISO phantom as noted by the arrowhead in the ISO-only images (Fig. 3c & 3e). ROI-based measurements (mean and standard deviation) of each phantom in the CSE images are shown directly in Fig. 3. The CSE reconstruction also showed effective spatial and spectral separation in mixed concentrations of PFCE and ISO (Fig. 4). Quantitatively, the measured PFCE and ISO signal levels were directly proportional to their known ^{19}F relative volumes in the mixed phantom (Fig. 4d). PFCE signal showed a linear behavior (R^2 = 0.987) with the known volume fraction, as expected.

In vivo results demonstrated that the accumulating ^{19}F ISO signal was detectable in the peritoneal cavity (Fig. 5a) and can be visualized by ^{19}F MRI (Fig. 5b). After intraperitoneal injection of PFCE, substantial dissolved fluorinated gas contamination can be observed in the source image compromising interpretation of the PFCE signal (Fig. 5d). CSE reconstruction demonstrates that the background ISO signal can be removed from ^{19}F MR images (Fig. 5d) enabling visualization of the PFCE alone. The PFCE emulsion signal was detected superior to the injection site with some of the emulsion spreading through the peritoneal cavity.

Corresponding ^{19}F spectra acquired with a non-selective RF pulse pre- and post-PFCE injection shows an absence of PFCE signal prior to injection with significant isoflurane accumulation in the first half hour of the experiment (Supporting Fig. S1a). After injection, a PFCE peak was observed in the ^{19}F spectrum with a gradual accumulation of ISO over the duration of the in vivo scan (Supporting Fig. S1b). An increase in the relative ^{19}F chemical shifts between PFCE and the two spectral groups of ISO was observed in vivo, compared to the in vitro results. The chemical shifts were measured to be 2.2 kHz (11.7 ppm) and 0.95 kHz (5.1 ppm), respectively and there were used as inputs into the signal model (Eq. 1).

Discussion

This work introduces a CSE approach to ^{19}F MR imaging of single-resonance perfluorocarbons that uses multi-spectral fluorine signal modeling with least-squares estimation to remove fluorinated anesthetic signal. Both 2D and 3D spoiled gradient-echo pulse sequences are used to demonstrate feasibility of the model-based CSE imaging approach to characterize complex spectra in ^{19}F MRI applied to removal of fluorinated anesthetic signal. Further, CRLB analysis is used to select acquisition parameters (TE_{init}, ΔTE, and N_{TE}) for improved signal-to-noise performance by maximizing the theoretical NSA_{eff}.

The CSE methodology proposed here provides the flexibility for applications that require chemical shift separation or selective quantification to separate multiple fluorine peaks using ^{19}F MRI. The fluorine peak from PFCE can be measured separately from peaks arising from ISO. Further, the multiple ISO peaks are inherently corrected for their chemical shift artifact by the k-space reconstruction. These multiple peaks are effectively superimposed for optimized SNR and enhanced image quality, void of chemical shift artifact. This capability to recombine the multiple fluorine peaks of ISO in a single CSE reconstructed image may improve the detection sensitivity at low concentrations. The removal of ISO background signal from ^{19}F MR images may be broadly applicable to additional perfluorocarbon agents that have resonant frequencies close to that of ISO's two spectral group including perfluorooctyl bromide (PFOB) and perfluoropolyether (PFPE) (5, 6). The additional chemical shift observed in vivo, compared to those observed for the neat formulations in vitro, between the PFCE and ISO spectral groups is a direct result of ISO accumulation within different chemical environments (e.g. adipose tissue) (20). Subsequent CRLB analysis using the in vivo chemical shifts showed high NSA_{eff} (>0.95) with the scan parameters (data not shown). The measured chemical shifts in vivo were used in the corresponding ^{19}F CSE image reconstruction of in vivo data.

Others have demonstrated the utility of "multi-color" ^{19}F MRI to image two chemically shifted fluorine contrast agents using chemical shift imaging (CSI) (21) or chemical shift selective (6) techniques, as well as the ability of CSE methods to image a single, complex ^{19}F compound without chemical shift artifacts (22). However, our proposed method enables tracking of multiple fluorine species simultaneously, without the need for separate and dedicated MR acquisitions and/or multiple infusions of different contrast agents. With our proposed approach, the number of fluorine species resolvable must be less than the N_{TE}, with well separated peaks.

^{19}F molecular MRI suffers from low SNR that potentially compromises the CSE image reconstruction. To improve ^{19}F MR sensitivity, very low rBW values were used for in vivo studies (18 kHz). Typically, the level of chemical shift artifact or B_0 field inhomogeneity determines the lower limit of the selected rBW. The k-space signal modeling approach (18) corrects for the large phase accumulation during the acquisition trajectory as a result of the chemical shift separation between fluorine species concurrent with low rBW. Further, inclusion of a B_0 field map estimation improved the CSE reconstruction and may greatly enhance ^{19}F MRI around areas of higher B_0 field inhomogeneity.

Our current approach depends on use of a gradient-echo acquisition. Importantly, 3D gradient-echo has both higher SNR-efficiency and no chemical shift in the slice direction compared to its 2D counterpart (23) and, therefore, may be better suited for CSE ^{19}F MRI. Alternative data acquisition strategies with even higher SNR-efficiency (e.g. bSSFP or FSE) (9, 22) are desirable and may enable further improvements of the proposed CSE approach. ISO and PFCE are both known to have altered transverse relaxation times based on both their compartment and chemical environments (20, 24). We have assumed negligible T_2* contributions in this work. Long T_2's have been reported for PFCE and PFCE-based emulsions between 25-536 ms (6, 25) and ISO in adipose tissue 281 ms (26). Accounting for T_2* in a CSE reconstruction model, as has been shown elsewhere in ^{1}H MRI applications (27), may improve in vivo quantification of ^{19}F concentrations. Additionally, reduction of the T_1 of the imaged ^{19}F species may also enable more rapid imaging and improve SNR efficiency. Recently, inclusion of lanthanides (e.g. gadolinium) or transition ions (e.g. iron) into ^{19}F label formulations has shown improvements in reducing the observed T_1 relaxation times, boosting the SNR efficiency (28-31). These advancements will further improve the proposed CSE approach with increased detection sensitivity of ^{19}F in regions of low signal intensity near the noise floor. Lastly, this work represents a proof-of-concept in a single animal study. Further testing and characterization is warranted in both phantoms and in vivo. This includes acquisition parameter optimization via

CRLB analysis using the observed in vivo chemical shifts and testing specific disease models where regional uptake of PFCE is expected.

In conclusion, we have demonstrated the feasibility of a CSE imaging approach for separation of anesthetic and contrast agent signals in ^{19}F MRI using acquisition parameters optimized for SNR, and direct k-space reconstruction with multispectral fluorine signal modeling. Robust reconstruction of spatially isolated spectral components in mixed concentration phantoms was demonstrated. The approach also appears to effectively remove signal contributions from isoflurane in ^{19}F MR images of PFCE in vivo based on qualitative observations pre- and post-injection of PFCE.

Acknowledgments

The authors thank Dr. Sandro Mecozzi and Alexa Barres for providing the PFCE emulsion for in vivo studies, as well as Beth Rauch and the Department of Medical Physics for core scan time to allow methods development. This work is supported in part by the University of Wisconsin Institute for Clinical and Translation Research (UW ICTR) NIH awards UL1TR000427 and TL1TR000429, Hyundai Hope On Wheels award 133-AAB3113, GE Healthcare, as well as the Swiss National Science Foundation grant PZ00P3-154719. The authors have no relevant conflicts of interest to disclose.

Reference

1. Temme S, Bonner F, Schrader J, Flogel U. 19F magnetic resonance imaging of endogenous macrophages in inflammation. Wiley Interdiscip Rev Nanomed Nanobiotechnol. 2012;4(3):329-43.
2. Srinivas M, Heerschap A, Ahrens ET, Figdor CG, de Vries IJM. (19)F MRI for quantitative in vivo cell tracking. Trends in biotechnology. 2010;28(7):363-70.
3. Gaudet JM, Ribot EJ, Chen Y, Gilbert KM, Foster PJ. Tracking the fate of stem cell implants with fluorine-19 MRI. PLoS One. 2015;10(3):e0118544.
4. Ludwig KD, Gordon JW, Bouchlaka MN, Capitini CM, Bednarz BP, Fain SB. In-vivo tracking of 19F-labeled natural killer cells with MRI in lymphoid tumor model. In Proceedings of the 22nd Annual Meeting of ISMRM, Milan, Italy. 2014:p.2813.
5. Constantinides C, Maguire ML, Stork L, Swider E, Srinivas M, Carr CA, et al. Temporal accumulation and localization of isoflurane in the C57BL/6 mouse and assessment of its potential contamination in 19 F MRI with perfluoro-crown-ether-labeled cardiac progenitor cells at 9.4 Tesla. J Magn Reson Imaging. 2016.
6. Jacoby C, Temme S, Mayenfels F, Benoit N, Krafft MP, Schubert R, et al. Probing different perfluorocarbons for in vivo inflammation imaging by 19F MRI: image reconstruction, biological half-lives and sensitivity. NMR Biomed. 2014;27(3):261-71.
7. Lockhart SH, Cohen Y, Yasuda N, Freire B, Taheri S, Litt L, et al. Cerebral uptake and elimination of desflurane, isoflurane, and halothane from rabbit brain: an in vivo NMR study. Anesthesiology. 1991;74(3):575-80.

8. van Heeswijk RB, Pellegrin M, Flogel U, Gonzales C, Aubert JF, Mazzolai L, et al. Fluorine MR Imaging of Inflammation in Atherosclerotic Plaque in Vivo. Radiology. 2015;275(2):421-9.
9. Reeder SB, Pineda AR, Wen Z, Shimakawa A, Yu H, Brittain JH, et al. Iterative decomposition of water and fat with echo asymmetry and least-squares estimation (IDEAL): application with fast spin-echo imaging. Magn Reson Med. 2005;54(3):636-44.
10. Reeder SB, Brittain JH, Grist TM, Yen YF. Least-squares chemical shift separation for (13)C metabolic imaging. J Magn Reson Imaging. 2007;26(4):1145-52.
11. Eggers H, Bornert P. Chemical shift encoding-based water-fat separation methods. J Magn Reson Imaging. 2014;40(2):251-68.
12. Reeder SB, McKenzie CA, Pineda AR, Yu H, Shimakawa A, Brau AC, et al. Water-fat separation with IDEAL gradient-echo imaging. J Magn Reson Imaging. 2007;25(3):644-52.
13. Reeder SB, Markl M, Yu H, Hellinger JC, Herfkens RJ, Pelc NJ. Cardiac CINE imaging with IDEAL water-fat separation and steady-state free precession. J Magn Reson Imaging. 2005;22(1):44-52.
14. Sharma SD, Artz NS, Hernando D, Horng DE, Reeder SB. Improving chemical shift encoded water-fat separation using object-based information of the magnetic field inhomogeneity. Magn Reson Med. 2015;73(2):597-604.
15. Dixon WT. Simple proton spectroscopic imaging. Radiology. 1984;153(1):189-94.
16. Glover GH, Schneider E. Three-point Dixon technique for true water/fat decomposition with B0 inhomogeneity correction. Magn Reson Med. 1991;18(2):371-83.
17. Reeder SB, Wen Z, Yu H, Pineda AR, Gold GE, Markl M, et al. Multicoil Dixon chemical species separation with an iterative least-squares estimation method. Magn Reson Med. 2004;51(1):35-45.
18. Brodsky EK, Holmes JH, Yu H, Reeder SB. Generalized k-space decomposition with chemical shift correction for non-Cartesian water-fat imaging. Magn Reson Med. 2008;59(5):1151-64.
19. Pineda AR, Reeder SB, Wen Z, Pelc NJ. Cramer-Rao bounds for three-point decomposition of water and fat. Magn Reson Med. 2005;54(3):625-35.
20. Wyrwicz AM, Conboy CB, Ryback KR, Nichols BG, Eisele P. In vivo 19F-NMR study of isoflurane elimination from brain. Biochim Biophys Acta. 1987;927(1):86-91.
21. Weise G, Basse-Lüsebrink TC, Kleinschnitz C, Kampf T, Jakob PM, Stoll G. In Vivo Imaging of Stepwise Vessel Occlusion in Cerebral Photothrombosis of Mice by 19F MRI. PLOS ONE. 2011;6(12):e28143.
22. van Heeswijk RB, Colotti R, Darçot E, Delacoste J, Pellegrin M, Piccini D, et al. Multi-echo chemical shift encoding (MECSE) for sensitive fluorine-19 MRI of complex spectra. Proceedings of the 25th Annual Meeting of ISMRM, Honolulu, HI, USA. 2017:p.489.
23. Bernstein MA, King KF, Zhou XJ. Signal Acquisition and K-Space Sampling. Handbook of MRI Pulse Sequences. Burlington: Academic Press; 2004. p. 367-442.
24. Dardzinski BJ, Sotak CH. Rapid tissue oxygen tension mapping using 19F inversion-recovery echo-planar imaging of perfluoro-15-crown-5-ether. Magn Reson Med. 1994;32(1):88-97.
25. Fox MS, Gaudet JM, Foster PJ. Fluorine-19 MRI Contrast Agents for Cell Tracking and Lung Imaging. Magnetic Resonance Insights. 2015;8(Suppl 1):53-67.
26. Evers AS, Haycock JC, d'Avignon DA. The potency of fluorinated ether anesthetics correlates with their 19F spin-spin relaxation times in brain tissue. Biochem Biophys Res Commun. 1988;151(3):1039-45.
27. Hernando D, Kramer JH, Reeder SB. Multipeak fat-corrected complex R2* relaxometry: theory, optimization, and clinical validation. Magn Reson Med. 2013;70(5):1319-31.

28. Neubauer AM, Myerson J, Caruthers SD, Hockett FD, Winter PM, Chen J, et al. Gadolinium-modulated 19F signals from perfluorocarbon nanoparticles as a new strategy for molecular imaging. Magn Reson Med. 2008;60(5):1066-72.
29. Schmid F, Höltke C, Parker D, Faber C. Boosting 19F MRI—SNR efficient detection of paramagnetic contrast agents using ultrafast sequences. Magnetic Resonance in Medicine. 2013;69(4):1056-62.
30. Kislukhin AA, Xu H, Adams SR, Narsinh KH, Tsien RY, Ahrens ET. Paramagnetic fluorinated nanoemulsions for sensitive cellular fluorine-19 magnetic resonance imaging. Nature materials. 2016.
31. de Vries A, Moonen R, Yildirim M, Langereis S, Lamerichs R, Pikkemaat JA, et al. Relaxometric studies of gadolinium-functionalized perfluorocarbon nanoparticles for MR imaging. Contrast Media Mol Imaging. 2014;9(1):83-91.

Figure Captions

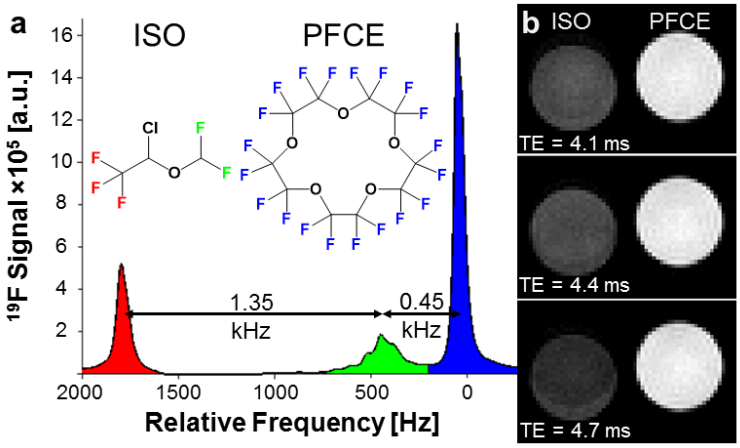

Figure 1. An MR spectrum showing the relative fluorine-19 (^{19}F) chemical shifts of PFCE and ISO at 4.7 T (**a**). The molecular structures of PFCE and ISO are color-coded according to their respective resonances. The consequence of these different resonances manifests as a chemical shift artifact observable in iFFT reconstructed MR images of physically aligned phantoms of PFCE and ISO displayed here at three different TEs (**b**).

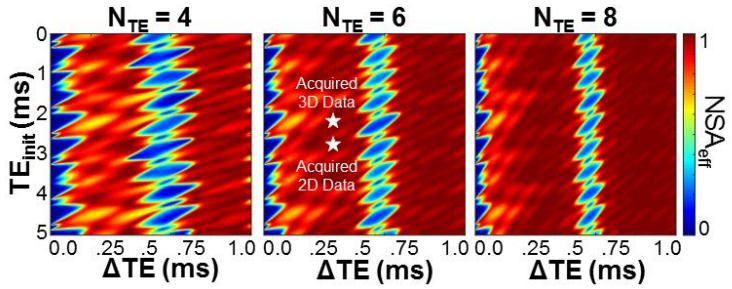

Figure 2. Noise performance for chemical shift encoded separation of PFCE and ISO is dependent on the echo time combination (TEs, TE_{init}, and ΔTE). In this work, 6 TEs were acquired with TE_{init} = 2.3 ms or 2.8 ms for 3D and 2D imaging, respectively, and ΔTE = 0.33 ms resulting in NSA_{eff}>0.95 for PFCE imaging (maximum NSA_{eff} is 1).

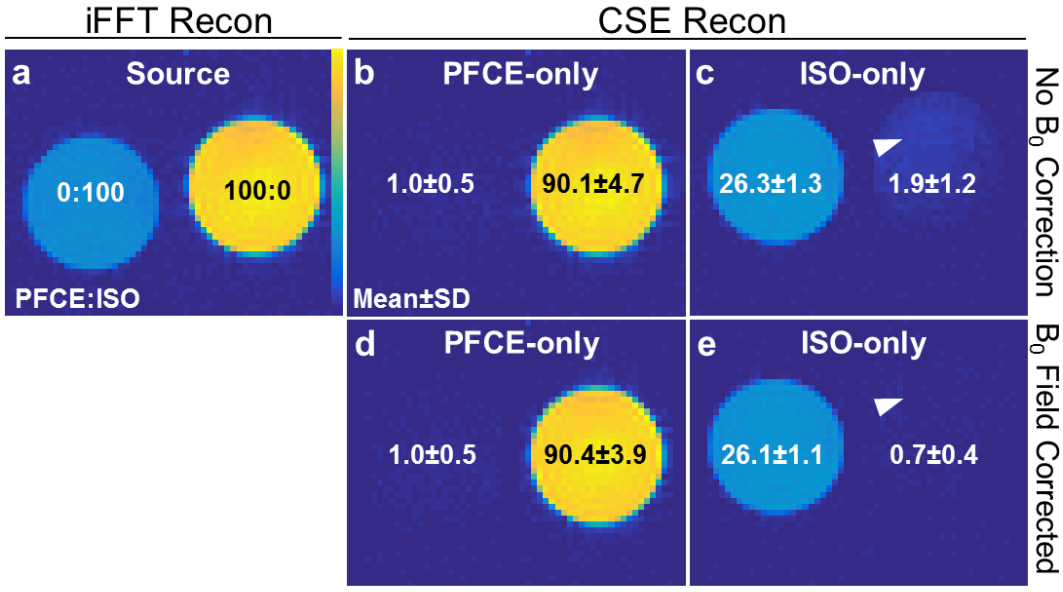

Figure 3. Feasibility of the chemical shift encoded (CSE) approach is demonstrated in ^{19}F MR images of PFCE and ISO phantoms reconstructed with either a conventional iFFT (**a**), listed here as 'source' image, or CSE image reconstruction of PFCE signal (**b,d**) and ISO signal (**c,e**). Reduced residual PFCE signal 'leakage' into ISO-only image (arrowheads) is noted when including the B_0 field estimation in the signal model. ROI-based measurements of mean ^{19}F signal ± standard deviation in PFCE and ISO phantoms for CSE reconstructed MR images are displayed directly on the figure.

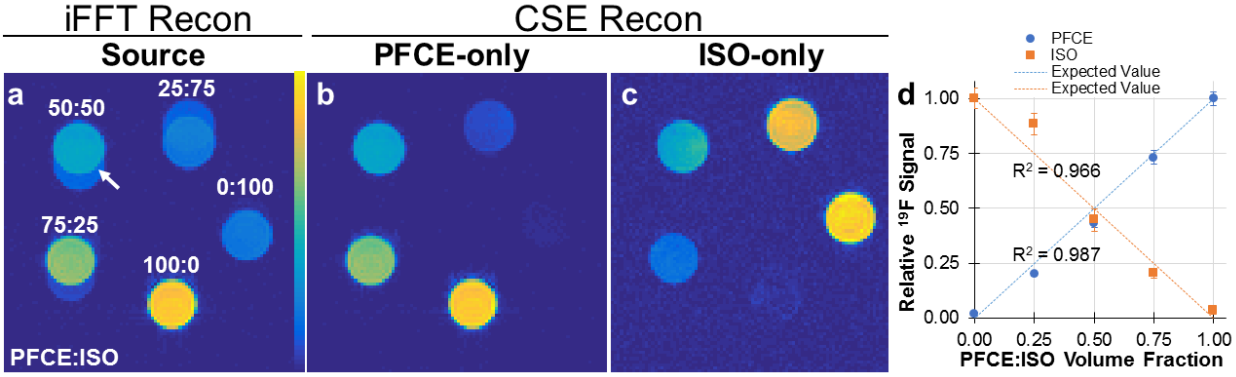

Figure 4. ^{19}F MR images of a phantom with mixed relative volumes of PFCE and ISO reconstructed with a conventional iFFT (**a**) shows chemical shift artifact (white arrow). The true PFCE:ISO volume fraction in each phantom is listed on the 'source' image. The CSE reconstruction demonstrates artifact-free signal recovery in the separate PFCE-only (**b**) and ISO-only images (**c**). The relative ^{19}F signal was measured from the PFCE-only or ISO-only CSE reconstructed images and plotted against the PFCE:ISO volume fraction (**d**). Dotted lines represent the expected signal intensities for the fluorine species based on the known volume fraction of PFCE:ISO. Error bars are included as the standard deviation of the measured signal within an ROI.

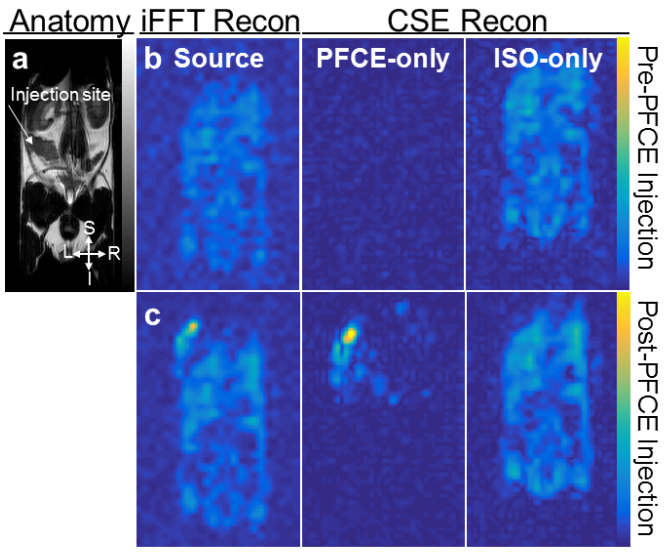

Figure 5. In vivo feasibility of CSE image reconstruction of PFCE with removal of background ISO signals is demonstrated in a healthy mouse. An anatomical reference image with the noted injection site (**a**) in gray scale is shown. ^{19}F MR images in color scale taken before (**b**) and after (**c**) intraperitoneal injection a PFCE emulsion, shows substantial isoflurane background signal in both source images pre- and post-PFCE injections. No PFCE signal was observed above the noise in the PFCE-only pre-injection image while PFCE signal is spread throughout the peritoneal cavity as seen in the PFCE-only post-injection image.

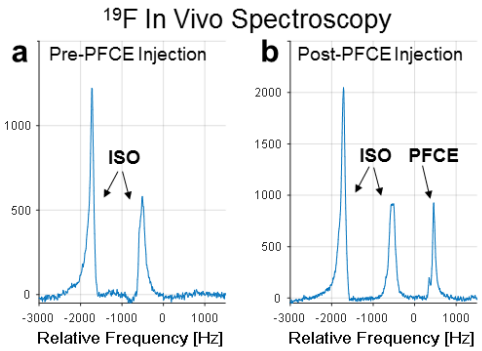

Supporting Figure S1. Non-selective ^{19}F spectra acquired pre- (**a**) and post- (**b**) PFCE injection showing the relative signal intensities observed for the PFCE and ISO spectral groups in vivo and used to empirically set the expected chemical shift frequencies for the signal model for image reconstruction.